Available online at www.sciencedirect.com

ScienceDirect

Procedia Structural Integrity 2 (2016) 2299–2306

Structural Integrity Procedia

www.elsevier.com/locate/procedia

21st European Conference on Fracture, ECF21, 20-24 June 2016, Catania, Italy

Microstructural changes during deformation of AISI 300 grade austenitic stainless steels: Impact of chemical heterogeneity

Jiří Man[a]*, Ivo Kuběna[a], Marek Smaga[b], Ondřej Man[c], Antti Järvenpää[d], Anja Weidner[e], Zdeněk Chlup[a], Jaroslav Polák[a]

[a]*Institute of Physics of Materials ASCR, Žižkova 22, 616 62 Brno, Czech Republic*
[b]*Institute of Materials Science and Engineering, University of Kaiserslautern, P.O. Box 3049, 67653 Kaiserslautern, Germany*
[c]*CEITEC, Brno University of Technology, Podnikatelská 6, 616 69 Brno, Czech Republic*
[d]*Centre for Advanced Steel Research, University of Oulu, 90014 Oulu, Finland*
[e]*Institute of Materials Engineering, TU Bergakademie Freiberg, Gustav-Zeuner-Str. 5, 09596 Freiberg, Germany*

Abstract

The present work points out the importance of chemical heterogeneity on the destabilization of austenitic structure and the formation of deformation induced martensite (DIM) in AISI 300 grade austenitic stainless steels (ASSs) of different level of austenite stability (316L, 304, 301LN). Color etching reveals that the structure of wrought Cr–Ni type steels is never fully chemically homogeneous. Confrontation of distribution and morphology of DIM formed in the volume of material after static and cyclic straining under well controlled different conditions with the characteristic local variations in chemical composition of diverse wrought semi-product forms (plates, sheets, bars) proved prominent and very important role of *chemical banding* in the destabilization of originally fully austenitic structure. This fact should be considered especially when interpreting the results of hydrogen embrittlement tensile testing of Cr–Ni ASSs with lowered Ni content. An impact of chemical heterogeneity on microstructural changes during production of UFG structure of 301LN and its cyclic straining is highlighted.

Peer-review under responsibility of the Scientific Committee of ECF21.

Keywords: wrought Cr–Ni austenitic stainless steels; deformation induced martensite; chemical banding; UFG structure; color metallography

* Corresponding author. Tel.: +420 532 290 383; fax: +420 541 218 657.
E-mail address: man@ipm.cz

Copyright © 2016 The Authors. Published by Elsevier B.V. This is an open access article under the CC BY-NC-ND license (http://creativecommons.org/licenses/by-nc-nd/4.0/).
Peer review under responsibility of the Scientific Committee of ECF21.
10.1016/j.prostr.2016.06.288

1. Introduction

The AISI type 300 (Cr–Ni) austenitic stainless steels (ASSs) constitute an important class of materials widely used in engineering practice at room, elevated and cryogenic temperatures (Lacombe et al. (1993), Lo et al. (2009)). The austenitic structure of these alloys is metastable, i.e. martensitic transformation γ→α' can occur during cooling and/or deformation (Lecroisey and Pineau (1972), Olson and Cohen (1972),Tamura (1982)); for a recent review see e.g. Lo et al. (2009) and Hedström and Odqvist (2015). Destabilization of austenite and formation of deformation induced martensite (DIM) still represent an important topic for these steels and is pursued at present from various standpoints: (i) perspective tool for the controlled strengthening (Spencer et al. (2004), Müller-Bollenhagen et al. (2010)), (ii) possible use for NDT monitoring of fatigue damage and/or assessment of residual fatigue life (Leber et al. (2007), Smaga et al. (2008)), (iii) magnetic stability (superconducting magnets) (Tobler et al. (1997)), (iv) the role of DIM in hydrogen environment embrittlement (HEE) (Michler et al. (2008, 2009), Weber et al. (2011), San Marchi (2012)) and (v) grain refinement via so called martensite-to-austenite reversion after previous cold deformation (see e.g. Poulon-Quintin et al. (2009), Sun et al. (2015), Misra et al. (2015), Behjati et al. (2016)).

The stability of ASSs depends primarily on the chemical composition and temperature – see two characteristic threshold temperatures calculated using empirically derived equations and designated as M_s and M_{d30} (Pickering (1978), Smaga et al. (2006) and Lo et al. (2009)). Although several very rare works indicated a prominent role of local chemistry on DIM formation in wrought AISI 300-grade steels deformed under various conditions (Lichtenfeld et al. (2006), Michler et al. (2008, 2009), Müller-Bollenhagen et al. (2010), Weber et al. (2011), Maréchal (2011)), in majority of present abundant studies this fact is either simply overlooked or not detected due to the incomplete structure characterization. Thus only the nominal chemical composition of steels is typically considered in these studies.

The aim of the present work is to show how the relatively small but specific variations in chemistry of wrought austenitic stainless steels can have an important effect on the mechanical destabilization of their structure. This is demonstrated on several working examples with steels of different austenite stability – 316L, 304 and 301LN deformed under various conditions. For this purpose diverse microscopic techniques were adopted including color etching technique to characterize distribution and morphology of DIM. The origin and extent of the characteristic chemical heterogeneity in the form of chemical banding is discussed in the context of the solidification behavior and contemporary steel production route. Distinctive role of inhomogeneous distribution of DIM in areas in which it should not be ignored hereafter are briefly pointed out.

2. Experimental

Chemical composition and the form of industrially produced steels together with two characteristic threshold temperatures M_s and M_{d30} calculated using empirical equations derived by Pickering (1978) are listed in Table 1. All steels except 301LN steel (see below) were tested in the solution-annealed state; grain size of fully austenitic structure was typically in the range 30–40 μm. Ferritoscopic measurements prior mechanical straining proved no detectable presence of δ-ferrite in the structure of ASS.

304 and 316L(N) steels were cyclically deformed under plastic strain control with low constant strain rate at room and depressed temperatures respectively (for further details see Smaga et al. (2006) and Man et al. (2011)). Smooth cylindrical specimens with the dimensions ∅4 × 24 mm were machined from central and circumferential part of 316L steel bar (see Table 1). Tensile tests were performed at 223 K with strain rate of 5×10^{-4} s^{-1}.

Table 1. Semi-product form, chemical composition (wt. %) and characteristic threshold temperatures M_s and M_{d30} of austenitic stainless steels.

	Semi-product form	C	Si	Mn	Cr	Ni	Mo	N	Cu	M_s	M_{d30}
AISI 316L(N)	25 mm thick plate	0.018	0.42	1.68	17.6	13.8	2.6	0.071	…	–367 °C	–126 °C
AISI 316L	bar, dia. 22 mm	0.015	0.41	1.66	16.5	10.05	2.03	0.025	…	–156 °C	–3 °C
AISI 304	bar, dia. 20 mm	0.030	0.58	1.75	18.42	9.05	0.37	0.05	0.03	–116 °C	0 °C
AISI 301LN	thin sheet (see the text)	0.017	0.52	1.29	17.3	6.5	0.15	0.15	0.2	–133 °C	35 °C

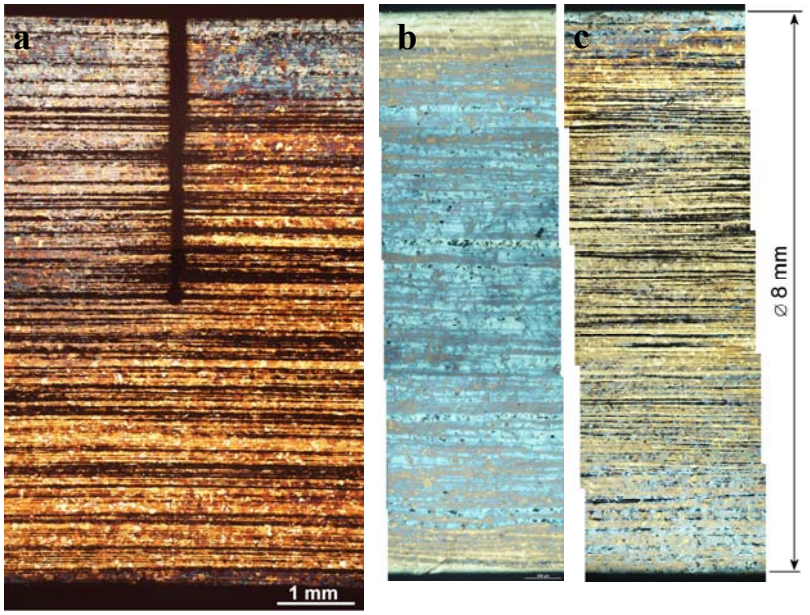

Fig. 1. Distribution of DIM in austenitic stainless steels fatigued to the end of fatigue life (Beraha II, OM). (a) 304 steel, $\varepsilon_{ap} = 6\times10^{-3}$, 293 K; (b) 316L(N) steel, $\varepsilon_{ap} = 2\times10^{-3}$, 143 K; (c) 316L(N) steel, $\varepsilon_{ap} = 2\times10^{-3}$, 113 K. Axial section of specimen, stress axis is horizontal.

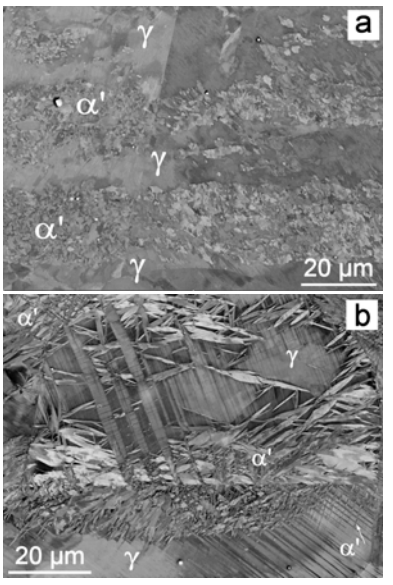

Fig. 2. Detail of morphology of DIM in fatigued (a) 304 and (b) 316L(N) steel. ECCI, SEM–FEG. Stress axis is horizontal.

301LN steel in the form of a thin sheet with ultrafine grain (UFG) size of 1.4 μm was produced by special thermo-mechanical treatment based on the martensite-to-austenite reversion annealing after cold working. LCF tests were performed at ambient temperature in tension-compression under total strain control with constant strain rate of 2×10^{-3} s^{-1}. Further details are given elsewhere (Chlupová et al. (2014)).

Testing specimens after completion of different tests were sectioned by spark erosion and carefully polished mechanically and electrolytically. Two color etching techniques have been adopted for characterization of microstructure of all austenitic stainless steels: Beraha II (BII) for detection and characterization of DIM and Lichtenegger and Bloech I (LBI) for visualization of chemical heterogeneity; for details see Weck and Leistner (1983). For a more detail study of microstructural changes ECCI (electron channeling contrast imaging) and EBSD (electron backscatter diffraction) techniques in high-resolution SEM–FEG (LYRA 3 XMU or MIRA 3 XMU from Tescan and FEI Verios 460L) were utilized. Local chemical analyses were performed in the line scan mode using EDS (energy dispersive spectroscopy).

3. Results and discussion

3.1. Case 1: LCF straining of 304 and 316L steels

The previous systematic study by Smaga et al. (2006) showed that constant plastic strain amplitude cyclic straining of 304 steel already at room temperature results in destabilization of originally fully austenitic structure. Figure 1a shows that DIM (= dark areas in Fig. 1) is not homogeneously distributed within the whole volume of the gauge part of the longitudinally sectioned specimen but instead bands of high and low DIM density running parallel to the rolling direction, irrespective of individual grain orientations, are clearly apparent. The same is true also for more stable 316L(N) steel fatigued however at depressed temperatures (c.f. Figs. 1b and 1c). Differences in the morphology of DIM detected in both steels under different temperatures are apparent from Fig. 2.

Whereas on the longitudinal sections of fatigued specimens the distribution of DIM always resembles band-like arrangement, completely different view on the distribution yields cross-sections perpendicular to the specimen axis, see Fig. 3. Depending on the form of semi-product used for fabrication of testing specimens two characteristic arrangements of DIM (= black features in Fig. 3) can be clearly recognized: (i) amoeba-shape in the case of

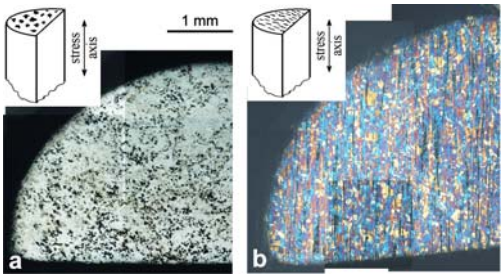

Fig. 3. Characteristic distribution of DIM on specimen cross-sections perpendicular to the stress axis. (a) 304 steel, $\varepsilon_{ap} = 6\times10^{-3}$, 293 K; (b) 316L(N) steel, $\varepsilon_{ap} = 2\times10^{-3}$, 113 K. BII etching, OM.

cylindrical bar (Fig. 3a) or (ii) lamellar shape in the case of thick plate (Fig. 3b). Comparing Figs. 1 and 3 the three-dimensional nature of DIM distribution in the material is apparent for both semi-products in agreement with the results by Michler et al. (2009).

3.2. Case 2: Tensile behavior of 316L steel at depressed temperatures: centre vs. periphery of bar product

Hydrogen embrittlement (HE) of Cr–Ni ASSs has been extensively studied for several decades (San Marchi (2012)). Small strain rate tensile (SSRT) tests using both internal and external hydrogen repeatedly confirmed that the degree of HE of these steels strongly depends on the nickel content. Effect of various metallurgical variables on HE has been monitored systematically, nevertheless the role of DIM has not been fully clarified yet. Recently Michler et al. (2008, 2009) performed an extensive comparative study on HE of ASSs using typical SSRT tests and it was firstly recognized that there is a difference in characteristic inhomogeneous distribution of DIM between the specimens machined from bars and plates in similar fashion shown in Figs. 1 and 3. This was attributed by the authors to macro-segregation of nickel.

Michler et al. (2008, 2009) in their studies unfortunately did not include the dimensions of the steel semi-product forms. As will be shown in detail elsewhere (Man et al. (2016)) any industrially produced ASS semi-product is, however, usually segregated remarkably only in its centre – see Fig. 4 showing homogeneity through the whole cross-section of 316L cylindrical bar with relatively low nickel content (see Table 1). To separate the effect of segregation on tensile behavior of the steel, tensile specimens were machined from both the central segregated area and as well as from the circumferential, more homogeneous part of the bar (data on local chemistry are given in part 3.4). The specimens were tensile deformed under similar parameters used in HE studies, i.e. at strain rate of 5×10^{-4} s^{-1} and 223 K. Although the stress-strain responses of both sets of specimens were practically congruent and ferritoscopic measurements showed identical content of DIM (50 vol.%), clear difference was revealed using color etching in the distribution of DIM after 30% tensile deformation – see darker features in Figure 5. Whereas the specimens taken from circumferential part of the bar show more or less relatively homogeneous distribution of DIM, the specimens taken from the central area indicate starting formation of prominent banded structure consisting of bands of high DIM density separated by strongly deformed austenite only with low density of DIM. Although we

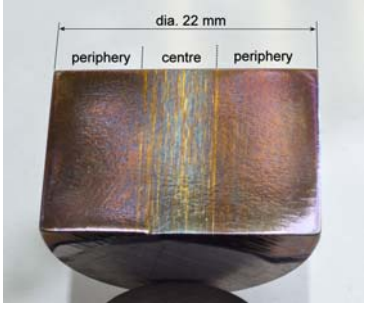

Fig. 4. Chemical heterogeneity inside 316L steel bar as revealed by LBI etching.

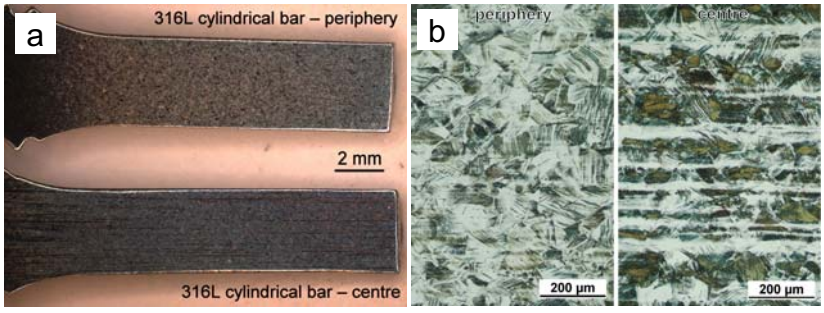

Fig. 5. Characteristic distribution of DIM in specimens taken from peripheral and central part of 316L steel bar after 30% tensile deformation at 223 K. (a) general overview of axially sectioned specimens, (b) detail of microstructure (BII etching, OM).

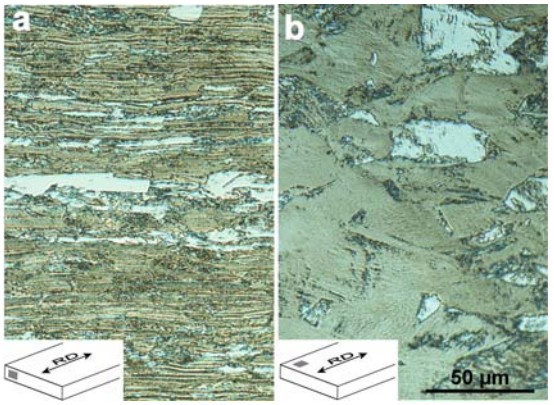

Fig. 6. Structure of 301LN steel after 70% cold rolling reduction revealed on (a) cross-section and (b) surface of the sheet using BII color etching (OM). RD = rolling direction.

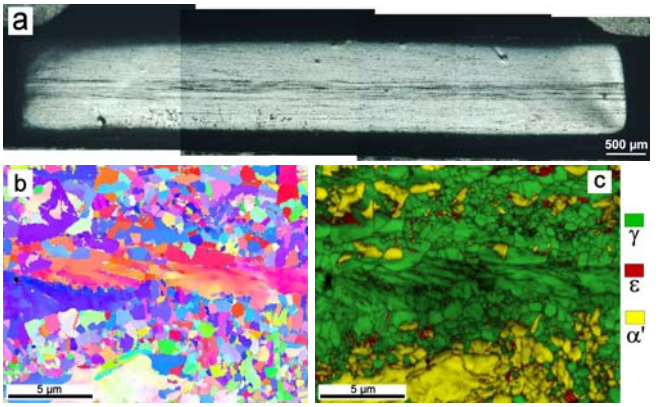

Fig. 7. 301LN steel with UFG structure cycled with $\varepsilon_{at} = 5\times10^{-3}$ to the end of fatigue life. (a) Overview of specimen cross-section (BII, OM), (b) inverse pole figure and (c) phase map obtained by EBSD from central part (a).

had no possibility to perform tensile test with hydrogen, this result indicates that also dimensions of ASSs semi-products and thus true extent of segregated area should be considered in HE studies (especially under external hydrogen).

3.3. Case 3: Production and LCF behavior of UFG 301LN stainless steel

The martensite-to-austenite reversion is known to be an effective tool for the grain refinement of metastable austenitic steels (see e.g. Poulon-Quintin et al. (2009), Sun et al. (2015), Misra et al. (2015), Behjati et al. (2016)). Depending on the degree of cold rolling (CR) and parameters of subsequent reversion annealing (temperature and time) various microstructural states can be obtained including so called UFG (ultrafine grained) structure. Austenitic steels with fully UFG structure across the sheet thickness is, however, generally achievable only for heavy CR reductions of 80–90% which are difficult to perform in industrial scale (for a recent review on this topic see Behjati et al. (2016)). Lower thickness reductions followed by proper reversion annealing were found to result in complex microstructure where UFG grains coexist with areas of coarser grains (i.e. bimodal structure) and sometimes with only partially recrystallized austenite. The reason for this microstructural heterogeneity has been discussed either in terms of different nature of DIM (lath-type vs. dislocation-cell type) (Misra et al. (2010)) or texture developing during cold-rolling process (Poulon-Quintin (2009)). Both findings are in principle true; however, as will be indicated bellow, they are only consequences of cold rolling of not fully chemically homogeneous austenitic steel sheet.

Figure 6 shows structure of 301LN steel sheet after CR reduction of 70%. As it is seen from this figure the austenite did not completely transform to DIM (darker areas in Fig. 6), neither on the sheet surface nor in the bulk of the sheet (c.f. Figs. 6a and 6b). Band–like character of DIM separated by the layers of heavily deformed austenite arrangement is clearly apparent in the central part of the sheet cross-section (Fig. 6a). Adopted reversion annealing 800 °C/1 s resulted in considerable grain refinement, nevertheless the structure both on the surface as well as inside the sheet showed some degree of grain bimodality and the presence of only partially transformed austenite (Chlupová et al. (2013)). Both these features are apparent from Fig. 7b which yields the view of the structure from the same perspective shown in Fig. 6a.

The 301LN steel sheets with bimodal-UFG fully austenitic structure and its coarse counterpart were cyclically strained at room temperature under low-cycle-fatigue conditions (Chlupová et al. (2014)). Whereas the coarse grained 301LN steel showed after LCF tests considerably inhomogeneous distributions of DIM through the whole specimen cross-section (not shown here), cyclic straining of the same steel with the bimodal-UFG grain structure yielded substantially different picture – see Fig. 7a. As can be seen from this figure the grain refinement resulted in considerably homogeneous distribution of DIM except the central part of the sheet where the effect of chemical banding inherited from the casting process (see below) persisted irrespective of fine grain size and thus nearly

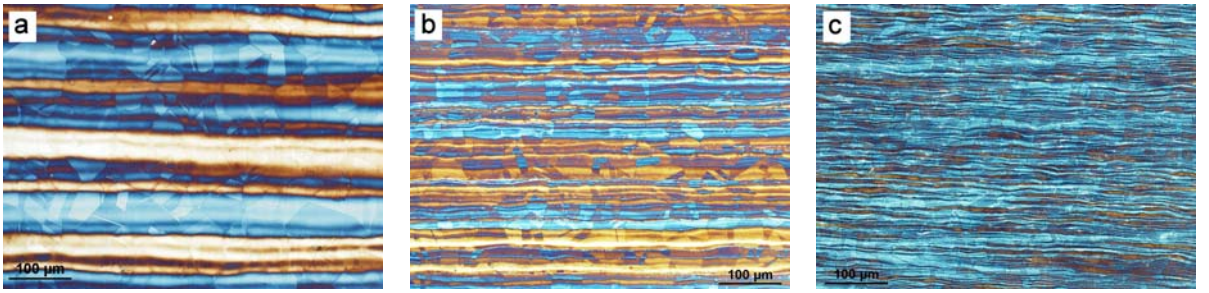

Fig. 8. Chemical banding in 316L type austenitic stainless steel as revealed by color etching (LBI) in central part of flat wrought products of different thickness: (a) 25 mm thick plate, (b) 5 mm thick strip, (c) 3 mm thick sheet. Rolling direction is horizontal in all micrographs, OM.

compact areas of DIM running parallel to the sheet surface and rolling direction can be detected in the steel structure (c.f. Figs. 7a and 7c).

3.4. Origin of chemical banding in Cr–Ni ASSs and its impact

Detailed discussion on the origin of distinctive inhomogeneous distribution of alloying elements aligned in fibers or plates parallel to the direction of working axis of long or flat products (i.e. bars or plates) respectively is beyond the scope of the present paper and will be published elsewhere (Man et al. (2016)). Here it can be briefly stated that its origin is principally the same as in the well-known case – i.e. ferrite/pearlite banding in hypoeutectoid steels, namely segregation during solidification (see e.g. Offerman et al. (2002), Krauss (2003)). In the case of ASSs studied in the present work the complex solidification sequence is followed by the so called solid-state transformation $\delta \rightarrow \gamma$ (Lacombe et al. (1993), Allan (1995)). Among other important factors influencing the intensity and extent of segregated area belong cooling rate, overall alloying level and the type of casting (ingot vs. continuous casting, laboratory-scale casting). Segregations within casted products (ingots, blooms or slabs) are during subsequent hot and cold working process aligned to the form of chemical banding and inherited to the final wrought structure – see Fig. 8. As it is clear from this figure the segregation bands of different thickness are running across the fully austenitic structure irrespective of the orientation of individual grains. Although an intensive working usually leads to the considerable 'homogenization' of final wrought semi-products, the chemical banding in their central parts is, however, persisting even after a very high working reduction levels, c.f. Figs. 4 and 8.

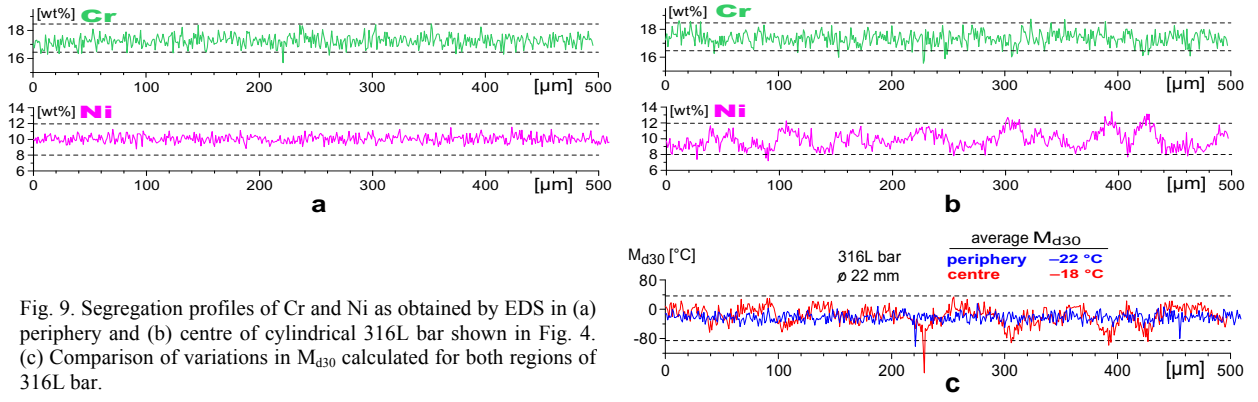

Fig. 9. Segregation profiles of Cr and Ni as obtained by EDS in (a) periphery and (b) centre of cylindrical 316L bar shown in Fig. 4. (c) Comparison of variations in M_{d30} calculated for both regions of 316L bar.

Inhomogeneous distribution of DIM well documented in the present paper for the Cr–Ni type ASSs steel in several working examples can be correlated with both the intensity and character of local variations of chemical composition (Man et al. (2016)). An example presents Fig. 9 which shows local variations in Cr and Ni determined by line scan EDS analysis in both peripheral and central area of longitudinally sectioned bar of 316L steel shown in Fig. 4. Results of the line analysis performed in both cases perpendicularly to the bar axis indicate clear difference

between both parts of the bar. The same analysis has been performed as well for other alloying elements, unfortunately, with the exception of carbon and nitrogen (Man et al. (2016)). Under premise that distribution of C and N is homogeneous in the whole volume, the profile M_{d30} temperature was calculated using Pickering's equations for both parts of the bar (Fig. 9c). Although the average temperatures M_{d30} are nearly identical for both parts, clear and not insignificant fluctuations are detectable in the central part of the bar. Their impact on the austenite destabilization in 316L steel tensile deformed at 223 K has been demonstrated in Fig. 5.

4. Conclusion

The present work showed that the wrought AISI 300-grade Cr–Ni austenitic stainless steels are never fully chemically homogeneous. Local chemical variations in the form of chemical banding aligned in fibers or plates running across the structure parallel to the direction of working axis irrespective of individual grain orientations are present in industrially produced long (bars or wires) or flat (plates, sheets and strips) products respectively. Since the stability (as well as stacking fault energy (SFE)) of austenite depends primarily on chemical composition and temperature (M_s, M_{d30}) these local, even very small, characteristic variations in steel chemistry will have an important effect on both distribution and morphology of deformation induced martensite. Although this fact may be irrelevant to the technical practice there are at least two areas where it should not be overlooked: the hydrogen embrittlement of ASSs with lowered nickel content and the production of UFG structure in metastable ASSs. Finally it should be highlighted that relatively old color etching techniques (Beraha II and Lichtenegger-Bloech I) still represent very sensitive and effective tools for microstructural characterization of Cr–Ni ASSs which under proper utilization serve to obtain results hardly achievable by other, even high-resolution techniques.

Acknowledgements

The support of the work by the project No. 13-32665S of the Czech Science Foundation is gratefully acknowledged. J.M. is indebted to Mrs. A. Macúchová from University of Žilina / Slovakia for her kind and helpful introduction into the mystique of color metallography.

References

Allan, G. K., 1995. Solidification of Austenitic Stainless Steels, Ironmaking and Steelmaking 22, 465–477.

Behjati, P., Kermanpur, A., Karjalainen, L. P., Järvenpää, A., Jaskari, M., Baghbadorani, H. S., Najafizadeh, A., Hamada, A., 2016. Influence of Prior Cold Rolling Reduction on Microstructure and Mechanical Properties of a Reversion Annealed High-Mn Austenitic Steels. Mater. Sci. Eng. A 650, 119–128.

Chlupová, A., Man, J., Polák, J., Karjalainen, L. P., 2013. Microstructural Investigation and Mechanical Testing of an Ultrafine-Grained Austenitic Stainless Steel, in *"NANOCON 2013"*. Tanger Ltd., Ostrava, pp. 733–738.

Chlupová, A., Man, J., Kuběna, I., Polák, J., Karjalainen, L. P., 2014. LCF Behaviour of Ultrafine Grained 301LN Stainless Steel. Proc. Eng. 74, 147–150.

Hedström, P., Odqvist, J., 2015. Deformation-Induced Martensitic Transformation in Metastable Austenitic Stainless Steels – Introduction and Current Perspectives, in *"Stainless Steel"*. In: Pramanik, A., Basak, A. K. (Eds.). Nova Science Publishers, Inc., New York, pp. 81–106.

Krauss, G., 2003. Solidification, Segregation, and Banding in Carbon and Alloy Steels. Metall. Mater. Trans. B 34B, 781–792.

Lacombe, P., Baroux, B., Beranger, G., 1993. *Stainless Steels*. Les Editions de Physique, Les Ulis.

Lecroisey, F., Pineau, A., 1972. Martensitic Transformations Induced by Plastic Deformation in the Fe-Ni-Cr-C System. Metall. Trans. 3, 387–396.

Leber, H. J., Niffenegger, M., Tirbonod, B., 2007. Microstructural Aspects of Low Cycle Fatigued Austenitic Stainless Tube and Pipe Steels. Mater. Charact. 58, 1006–1015.

Lichtenfeld, J. A., Mataya, M. C., van Tyne, C. J., 2006. Effect of Strain Rate on Stress-Strain Behavior of Alloy 309 and 304L Austenitic Stainless Steel. Metall. Mater. Trans. A 37, 147–161.

Lo, K. H., Shek, C. H., Lai, J. K. L., 2009. Recent Developments in Stainless Steels. Mater. Sci. Eng. R 65, 39–104.

Man, J., Obrtlík, K., Petrenec, M., Beran, P., Smaga, M., Weidner, A., Dluhoš, J., Kruml, T., Biermann, H., Eifler, D., Polák, J., 2011. Stability of Austenitic 316L Steel Against Martensite Formation During Cyclic Straining. Proc. Eng. 10, 1279–1284.

Man, J., Kuběna, I., Klusák, J., Polák, J., 2016. Chemical Banding in Wrought Cr—Ni Austenitic Stainless Steels. Part 1: Visualization and Quantitative Assessment of Chemical Heterogeneity in Different Steel Product Forms. Mater. Sci. Technol., to be published.

Maréchal, D., 2011. *Linkage Between Mechanical Properties and Phase Transformations in a 301LN Austenitic Stainless Steel.* PhD Thesis. The University of British Columbia, Vancouver, p. 129.

Michler, T., Naumann, J., 2008. Hydrogen Environment Embrittlement of Austenitic Stainless Steels at Low Temperatures. Int. J Hydrogen Energy 33, 2111–2122.

Michler, T., Lee, Y., Gangloff, R. P., Naumann, J., 2009. Influence of Macro Segregation on Hydrogen Environment Embrittlement of SUS 316L Stainless Steel. Int. J Hydrogen Energy 34, 3201–3209.

Misra, R. D. K., Wan, X. L., Challa, V. S. A., Somani, M. C., Murr, L. E., 2015. Relationship of Grain Size and Deformation Mechanism to the Fracture Behavior in High Strength-High Ductility Nanostructured Austenitic Stainless Steels. Mater. Sci. Eng. A 626, 41–50.

Müller-Bollenhagen, C., Zimmermann, M., Christ, H.-J., 2010. Very High Cycle Fatigue Behaviour of Austenitic Stainless Steel and the Effect of Strain-Induced Martensite. Int. J Fatigue 32, 936–942.

Offerman, S. E., van Dijk, N. H., Rekveldt, M. Th., Sietsma, J., van der Zwaag, S., 2002. Ferrite/Pearlite Band Formation in Hot Rolled Medium Carbon Steel. Mater. Sci. Technol. 18, 297–303.

Olson, G. B., Cohen, M., 1972. A Mechanism for the Strain-Induced Nucleation of Martensitic Transformations: J. Less-Common Metals 28, 107–118.

Pickering, F. B., 1978. Physical Metallurgy and the Design of Steels. Applied Science Publishers Ltd, London.

Poulon-Quintin, A., Brochet, S., Vogt, J.-B., Glez, J.-C., Mithieux, J.-D., 2009. Fine Grained Austenitic Stainless Steels: The Role of Strain Induced α' Martensite and the Reversion Mechanism Limitations. ISIJ Int. 49, 293–301.

San Marchi, C., 2012. Hydrogen Embrittlement of Austenitic Stainless Steels and Their Welds, in *"Gaseous Hydrogen Embrittlement of Materials in Energy Technologies, Volume 1: The Problem, Its Characterisation and Effects on Particular Alloy Classes"*. In: Gangloff, R. P., Somerday B. P. (Eds.). Woodhead Publishing Limited, Cambridge, UK, pp. 592–623.

Smaga, M., Walther, F., Eifler, D., 2006. Investigation and Modelling of the Plasticity Induced Martensite Formation in Metastable Austenites. Int. J. Mat. Sci. (formerly Z. Metallkd.) 97, 1648–1655.

Spencer, K., Embury, J. D., Conlon, K. T., Véron, M., Bréchet, Y., 2004. Strengthening via the Formation of Strain-Induced Martensite in Stainless Steels. Mater. Sci. Eng. A 387–389, 873–881.

Sun, G.S., Du, L. X., Hu, J., Xie, H., Wu, H. Y, Misra, R. D. K., 2015. Ultrahigh Strength Nano/Ultrafine-Grained 304 Stainless Steel Through Three-Stage Cold Rolling and Annealing Treatment. Mater. Charact. 110, 228–235.

Tamura, I., 1982. Deformation-Induced Martensitic Transformation and Transformation-Induced Plasticity in Steels. Metal Sci. 16, 245–253.

Tobler, R. L., Nishimura, A., Yamamoto, J., 1997. Design-Relevant Mechanical Properties of 316-Type Steels for Superconducting Magnets. Cryogenics 37, 533–550.

Weber, S., Martin, M., Theisen, S., 2011. Lean-Alloyed Austenitic Stainless Steel with High Resistance Against Hydrogen Environment Embrittlement. Mater. Sci. Eng. A 528, 7688–7695.

Weck, E., Leistner, E., 1983. Metallographic Instructions for Colour Etching by Immersion. Part II: Beraha Colour Etchants and Their Different Variants. DVS, Düsseldorf.